LBNL-44442
Preprint

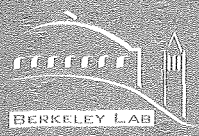

ERNEST ORLANDO LAWRENCE
BERKELEY NATIONAL LABORATORY

A Geometric Level Set Model for Ultrasounds Analysis

A. Sarti and R. Malladi

Computing Sciences Directorate
Mathematics Department

October 1999

To be submitted
for publication

LBNL-44442

A Geometric Level Set Model for Ultrasounds Analysis

A. Sarti and R. Malladi

Computing Sciences Directorate
Ernest Orlando Lawrence Berkeley National Laboratory
University of California
Berkeley, California 94720

October 1999

This work was supported by the Director, Office of Science, Office of Advanced Scientific Computing Research, Mathematical, Information, and Computational Sciences Division, of the U.S. Department of Energy under Contract No. DE-AC03-76SF00098.

A Geometric Level Set Model for Ultrasounds Analysis *

A. Sarti and R. Malladi

Mail Stop: 50A-1148, 1 Cyclotron Road
Lawrence Berkeley National Laboratory
University of California
Berkeley, California 94720.
{asarti,malladi}@math.lbl.gov

October 20, 1999

Abstract

We propose a partial differential equation (PDE) for filtering and segmentation of echocardiographic images based on a geometric-driven scheme. The method allows edge-preserving image smoothing and a semi-automatic segmentation of the heart chambers, that regularizes the shapes and improves edge fidelity especially in presence of distinct gaps in the edge map as is common in ultrasound imagery. A numerical scheme for solving the proposed PDE is borrowed from level set methods. Results on human in vivo acquired 2D, 2D+time,3D, 3D+time echocardiographic images are shown.

1 Introduction

Infarction of the heart muscle is the primary cause of death among human beings compared to all the other diseases. Therefore, evaluation of the heart functionality is an important component in good health care. Echocardiography is by far the most commonly used imaging technique to diagnose pathologies of the cardiac muscle. The features that have made it so largely used are its noninvasiveness, ease of use, low cost and effectiveness in diagnosing heart pathologies. $2D$ echocardiography only allows visualization of planar tomographic sections of the heart; thus, it relies on strong geometrical assumptions for the determination of heart chamber volume and is is subject to considerable measurement error, especially for the right ventricular and atrial volume determination [3]. On the other hand, $3D$ echocardiography overcomes the need for geometrical

*Supported in part by the Applied Mathematical Sciences Subprogram of the Office of Energy Research, U.S. Dept. of Energy under Contract DE-AC03-76SD00098, and LBNL Directed Research and Development Program.

assumptions, thereby allowing accurate evaluation of chambers size and shape, even in case of cavities with irregular geometry.

A serious drawback is the poor quality of echograms if compared, for example, with computed tomography (CT) or magnetic resonance (MR). An accurate visualization and interpretation of ultrasounds images is often affected by the high amount of noise intrinsically linked to the acquisition method. Indeed the process of formation of an ultrasound image involves a combination of coherent, rayleigh and diffractive scattering that produces the characteristic speckle-noise distribution [31]. Traditional pre-processing algorithms such as moving average, median and Gaussian filtering reduce the noise superimposed on the image but do not preserve the edge information or the boundaries [10]. Non-linear filtering methods based on partial differential equations have been applied in [18, 9, 26].

Many techniques have been proposed in the literature to extract the ventricular surface in conditions of end-systole and end-diastole – thus when the ventricle is closed – starting from a small number of $2D$ images that represent different sections of the ventricle. Reconstruction of the ventricular chamber has been widely studied in recent years from Computed Tomography and Magnetic Resonance Imaging. Cohen in [6][7] uses the concept of active deformable contours for the segmentation of ventricular shapes from $2D$ echocardiography and $3D$ magnetic resonance. The approach is a generalization of Kass, Witkin, and Terzopoulos deformable elastic model [12]. Malladi, Sethian, and Vemuri in [13, 14] combine the idea of deformable surfaces with the level-set approach of Osher and Sethian [20], by representing the surface as a particular level-set of an implicit function and applying it to the reconstruction of the ventricular chamber in $3D+$ time MR images; see [16].

The difficulty in segmenting the heart chamber shapes from echocardiograms is two fold; first, the images are relatively noisier resulting in poor edge indicator and second, due to opening and closing of the heart valve, the boundary of the left ventricle remains uncertain in some images. Big 'holes' due to open valve many times causes the shape model to erroneously flow into the atrium. We address both these issues in this paper. The noise and poor edge quality is handled with an edge preserving filtering mechanism [32] and the issue of shape uncertainty is resolved by exploiting the continuity assumption in time [26].

In this paper we want to address both the tasks of edge preserving image denoising and shape extraction of the cardiac chambers from echocardiographic images, by using the same geometric partial differential equation (PDE) based model. Encouraged by the recent advances [14][15] [16]-[17][32][2][23] [26][18] in PDE based image analysis tools, we extend and apply some of those methods to echocardiographic image analysis. The theme of this paper is to start with a governing equation that is expressed via an Euler-Lagrange of a functional and to show its many interpretations. A numerical scheme based on the level set methods [20] and the efficient narrow-band versions [1][14] of it are used to solve the main equation.

Another key aspect of this paper is the accurate computation of ventricular volume from the extracted shapes. This leads to the estimation of such quantities as ejection fraction from a time varying set of $3D$ images. Finally, to demonstrate the accuracy of our segmentation scheme, we compare the volume figures we obtain from segmenting sheep heart images to the exact experimentally measured values [PINI reference].

The rest paper is organized as follows: In Section 2 we present the main equation and we outline its relevant features. In Section 3 we interpret the main equation as an image processing algorithm and show its application in echocardiographic image denoising. In Section 4 we study the geometric interpretation of the model for shape segmentation. In Section 5-8 results of the application of the model to in vivo ultrasounds acquisitions are presented and details of the implementation are provided.

2 The geometric evolution equation

Consider an hypersurface $\Upsilon(x,t)$ that is propagating under the speed $\mathcal{F}$ in the normal direction. The speed $\mathcal{F}(N,\mathcal{K},x)$ is a function of the intrinsic geometrical properties of the hypersurface, like the normal vector and curvature, as well as of the position. We consider a level set equation [20][28][29] to represent this motion by embedding the hypersurface as the zero level-set of an higher dimensional function $\Psi(x,t)$, namely the set $\{\Psi(x,t)=0\}$. By following chain rule, the equation of motion of the embedding is

$$\Psi_t + \mathcal{F}|\nabla\Psi| = 0 \tag{1}$$

with the initial condition $\Psi(x, t = 0) = \Psi_0$. By embedding the evolution of $\Upsilon(x, t)$ in the evolution of of $\Psi(x, t)$, topological changes of $\Upsilon(x, t)$ are handled automatically and a numerical solution for the evolutionary hypersurface can be accurately achieved in the viscosity framework presented in [20]. Several applications in shape modeling have been presented using this model for surface propagation in [13][4][14][16]. Level set methods in image analysis have been introduced in [14] for boundary extraction. The method relies on evolving an initial manifold in the image domain and to mold the shape into the desired boundary. The key is a suitable design of the evolution speed $\mathcal{F}$. In [14] the speed function used to control the shape recovery process is a combination of constant inflationary speed, an intrinsic geometric speed that regularizes the final result and a speed that depends on the image:

$$\mathcal{F} = g\left(1 - \epsilon\nabla \cdot \frac{\nabla\Psi}{|\nabla\Psi|}\right) \tag{2}$$

where g is a decreasing function of the image gradient. It has to be noted that the curvature of the hypersurface written as a function of the level set of $\Psi(x, t)$ is just $\mathcal{K} = \nabla \cdot \frac{\nabla\Psi}{|\nabla\Psi|}$ and then the above expression defines the propagation of $\Upsilon(x, t)$ driven by the image features and regularized by the curvature; $\mathcal{K}$ is the Euclidean curvature for plane curves and the mean curvature for manifolds.

In addition to the speed term in Eqn. 2, an attraction to the boundary features can be defined by adding a forcing term that advects the surface along an image dependent vector field [5][16]. The vector field has to be synthesized such that it always points towards towards the local edge. The speed function then takes the form:

$$\mathcal{F} = g\left(1 - \epsilon\mathcal{K}\right) - \beta\nabla g \cdot \left(\frac{\nabla\Psi}{|\nabla\Psi|}\right), \tag{3}$$

where the unit normal to the surface is expressed by the term $N = -\frac{\nabla\Psi}{|\nabla\Psi|}$. The corresponding surface evolution has a steady state solution when the inflationary and the geometry dependent terms balance the advection term. As shown in [5, 16], this model of surface evolution leads to stable shape recovery even in the presence of minor gaps and oscillations along the edge. However, echocardiographic images are significantly noisier with much poorer edge definition when compared to CT, and MR images. They not only have noisy structures but often large parts of the boundaries are missing making the shape recovery really troublesome. So, even with the extra forcing term in Eqn. 3, the evolving "edge-seeking" surface can easily go through the gaps present in the edge map.

We aim to develop a filtering and segmentation method that deals with non-continuous edges.

We propose the following evolution equation for the level set function Ψ:

$$\Psi_t - g\mathcal{K}|\nabla\Psi| - \beta\nabla g \cdot \nabla\Psi = 0. \tag{4}$$

Notice that the constant component of the speed, i.e. the 'edge-seeking" term has been dropped. The reason for this change is two fold: (a) given a good initial condition, the segmentation algorithm will recover shapes with significant gaps by simply minimizing distance in areas where edge information is absent, and (2) as we show in the next section, the above equation can be used to denoise the original image as well as enhance edges. The edge enhancement step is used as a precursor to segmentation. The equation itself can be solved with user-defined initial condition during the segmentation step and with the original image as an initial condition for the edge-enhancement stage. The model regularizes the the boundaries where a clear representation of the edges is missing. It presents topological adaptability, robust numerics and very fast implementations [17].

3 The shock-type filtering

Low level image processing tends to achieve the basic result of computing a decomposition $\{\Omega_i\}$ of the domain $\Omega = \Omega_1 \cup \ldots \cup \Omega_N$ and computing an enhanced image similar to the original one, that varies smoothly and slowly within each Ω_i and discontinuously on (part of) the boundary of the Ω_i. Boundaries of the homogeneous regions Ω_i that are not part of the boundary of Ω are called edges[1]. The goal is then to smooth all the homogeneous regions that contain noise and to retain in an accurate way the location of the edges that define the shape of the represented structures. We shall now show how we can use Eqn 4 to do image processing. Let us consider an image $I_0(x) : \Omega \rightarrow$, where $\Omega \subset R^N$ is a rectangular spatial domain and $N = 2$ for $2D$ images and $N = 3$ for $3D$ images. The image filtering associates with $I_0(x)$ a family $\Psi(x,t) : \Omega \times [0,T] \rightarrow R$ of simplified-filtered images depending on an abstract parameter t, the *scale*. To better understand the method, let us consider the main equation, namely:

$$\Psi_t = g\left(\nabla \cdot \frac{\nabla\Psi}{|\nabla\Psi|}\right)|\nabla\Psi| + \beta\nabla g \cdot \nabla\Psi$$

$$g(x) = \frac{1}{1 + (|\nabla G_\sigma(x) \star I_0(x)|/\alpha)^2}$$

$$G_\sigma(\xi) = \frac{\exp(-(\xi/\sigma)^2)}{\sigma\sqrt{\pi}} \tag{5}$$

with the initial condition given by the noisy image $\Psi(x, t = 0) = I_0(x)$.

The first (parabolic) term in Eqn. 5 is a geometric diffusion term weighted by the edge indicator g. The geometric diffusion term $\left(\nabla \cdot \frac{\nabla\Psi}{|\nabla\Psi|}\right)|\nabla\Psi|$ is a degenerate diffusion term that diffuses the signal only in the direction parallel to the boundaries and not at all in the direction of $\nabla\Psi$ thereby preserving edge definition. Writing the diffusion term as Morel and Solimini noted that:

$$\left(\nabla \cdot \frac{\nabla\Psi}{|\nabla\Psi|}\right)|\nabla\Psi| = \Delta\Psi - \frac{D^2(\nabla\Psi, \nabla\Psi)}{|\nabla\Psi|^2} \tag{6}$$

Morel and Solimini noted that the first term, the Laplacian, is the same as in Scale Space Theory [2] and the second one is an inhibition of the diffusion in the direction of the gradient. The weighting function g enforces edge preservation by slowing down the geometric diffusion in presence of high gradient in the smoothed image. Thus the aim of the selective geometric diffusion term is to make Ψ smooth away from the edges with a minimal smoothing of the edge itself. The second (hyperbolic) term in Eqn 5 sharpens the edges by advecting the brightness signal of the initial image I_0 toward the edges following the vector fields induced by ∇g. A similar observation was made in [24].

The edge indicator $g(x)$ is a non-increasing function of $\nabla G_\sigma(x) \star I_0(x)$. To interpret this term we observe that the convolution property $\nabla G_\sigma(x) \star I_0(x) = \nabla(G_\sigma(x) \star I_0(x)) = G_\sigma(x) \star \nabla I_0(x)$ holds. Thus we can consider it as the gradient of a smoothed version of the initial image: $I_s(x) = G_\sigma(x) \star I_0(x)$. We compute it via heat-flow (an idea usually attributed to Koendrink) by observing that the convolution of the signal with Gaussian is equivalent to the solution of the heat equation:

$$\begin{aligned} I_s(x,t) &= \int_0^\sigma \Delta I(x,t)dt \\ I(x,0) &= I_0(x). \end{aligned} \tag{7}$$

In the filtering process the minimal size of the details that are preserved is related to the size of the Gauss kernel, which acts like a scale parameter. Notice that the filtering model reduces to mean curvature flow when $g(s) = 1$.

We have applied the multiscale analysis model to an in vivo acquired $2D$ and $3D$ echocardiographic sequence. The sequence has been obtained by means of a rotational acquisition technique

using the TomTec Imaging System. With this technique the transducer undergoes a rotation around its main axis in a propeller configuration. A series of tomographies corresponding to the sections of a cone of biological tissue have been acquired. The acquisition consists of 14 image-cubes that represent a whole cardiac cycle of a real patient. A volume of size 151 x 151 x 101 voxels has been processed. The interval of time between one $3D$ image and the next one is 40 ms.

In Figure 1 a slice of the $3D$ volume has been visualized. The original noisy image is shown on the left and the result of the multiscale denoising algorithm with $\alpha = 0.1, \beta = 1.5, \Delta t = 0.05$, and $\sigma = 0.001$ is presented on the right. In Figures 2–5 a sequence of filtered volumes is shown. The parameters are the same as in the $2D$ computation. The iso-surfaces corresponding to the interface between cardiac muscle and blood have been computed using the marching cubes method and visualized by a Gouraud surface rendering ([11], [30]). To clarify the visualization of the ventricular chambers we applied four cutting planes that isolate the region of interest. In clinical practice a cutting plane that filters out the "front" regions is often used. The epicardium is not visible because the gray levels of his interface are not captured by the marching cubes threshold we have chosen in order to visualize the left ventricle. In particular the low echogenicity of the blood allows the choice of a low isosurface threshold that avoids the visualization of most of the other structures.

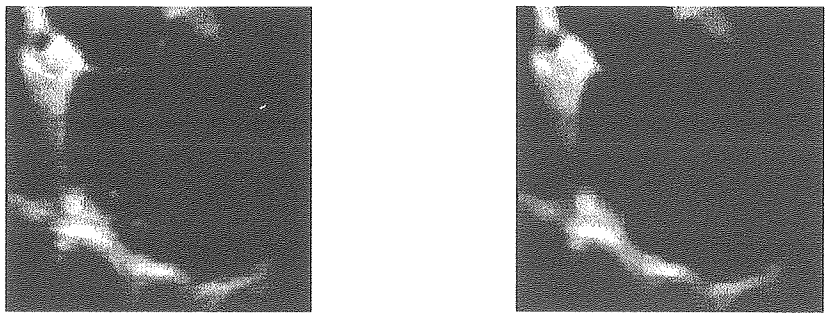

a) b)

Figure 1: *$2D$ echocardiography of in vivo acquired left ventricle. Left: original image. Right: result of geometric image denoising.*

Note that the $3D$ pictures are simply meant to visually demonstrate the degree of noise reduction via the proposed geometric method. A more thorough study involving measuring the degree of noise

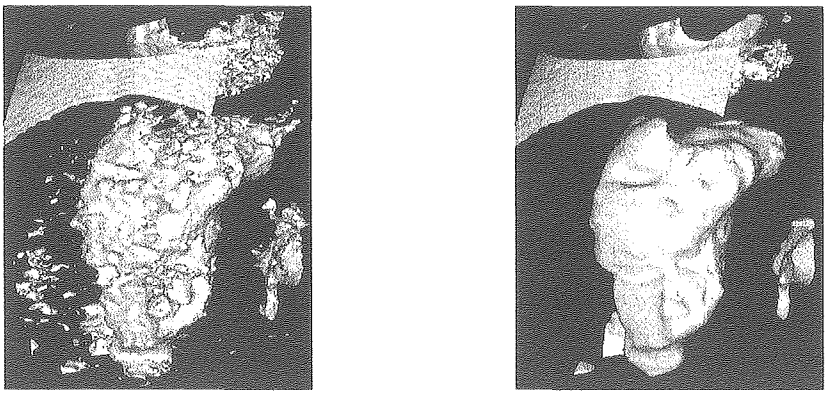

a) b)

Figure 2: *Geometric smoothing of the 1st frame of the 3D echocardiographic sequence.*

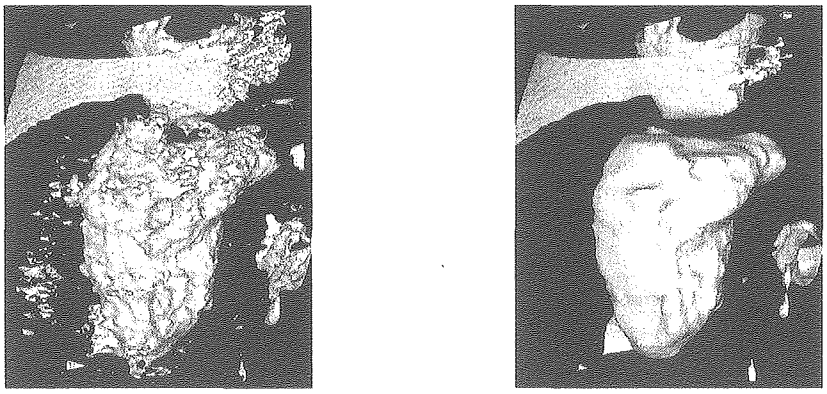

a) b)

Figure 3: *Geometric smoothing of the 5th frame of the 3D echocardiographic sequence.*

reduction and a detailed comparison with other denoising schemes has been done in another work [27]. The rendered surfaces can not be used for any measurement or tracking. The problem of explicitly building a shape model of the shape of interest is the topic of next section.

4 Shape extraction

Imagine a planar curve C_0 in an image $I(x) : \Omega \to R^+, \Omega \subset R^N, N = 2$, and consider the evolution $C(t)$ of that initial shape. We want to study the evolution rules that allows us to mold the curve conformally into the edge map. Consider first the basic motion:

$$C_t = F\mathbf{N} \tag{8}$$

a) b)

Figure 4: *Geometric smoothing of the 9th frame of the 3D echocardiographic sequence.*

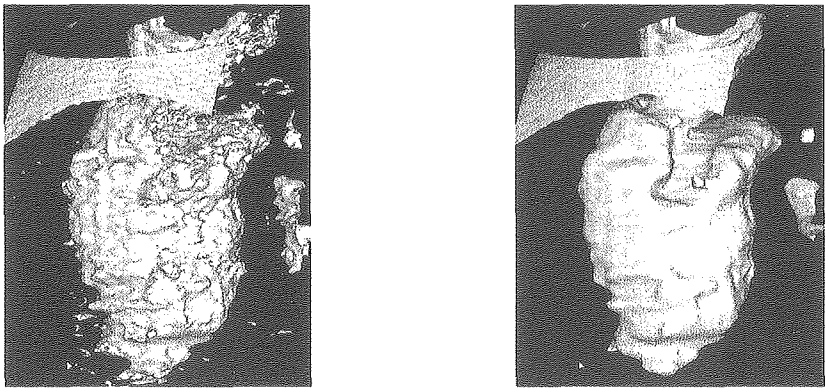

a) b)

Figure 5: *Geometric smoothing of the 13th frame of the 3D echocardiographic sequence.*

where $\mathbf{N}$ is the unit inward normal and F is a real function. The curve moves with speed F in the normal direction. Let us design F in such a way that $C(t)$ is attracted by the boundaries in the image. Consider the following evolution equation:

$$C_t = (-\nabla g \cdot \mathbf{N})\mathbf{N}. \tag{9}$$

Recall that the minima of the edge indicator $g(x)$ denote the position of the edges and therefore the vector field field $-\nabla g$ can be shown to point toward the edges. The result of this flow is an oscillatory curve without "smoothness" or regularization.

One way of introducing smoothness in the curve is to let it evolve under its Euclidean curvature

K,

$$C_t = K\mathbb{N}. \tag{10}$$

This flow decreases the Euclidean curvature and has the property of smoothing all the high curvature regions of the curve, i.e. the local variations [8]. However, this flow will also destroy useful curve features if run long enough. Thus a key point is to determine a suitable stopping criterion. Several methods have been proposed in the past in teh framework of variational methods [19] and level set methods [15]. The authors in [15] have presented a scale-dependent stopping criteria implemented via a min-max curvature flow. In the present context we use the function g to introduce the stopping criterion. Therefore the evolution equation for curve regularization becomes:

$$C_t = gK\mathbb{N} \tag{11}$$

where the curvature motion is slowed down in near the shape boundaries. The final evolution equation for shape extraction will use both the attraction and the regularization terms, namely

$$C_t = (gK - \beta(\nabla g \cdot \mathbb{N}))\mathbb{N} \tag{12}$$

where the initial condition $C(0) = C_0$ is any curve sufficiently close to the boundary to feel the effect of the edge map $g(x)$.

In [16, 17], the above curve evolution model has been extended to surface evolution for segmentation of $3D$ shapes from volumetric images. In this case we define a surface S_0 in an image $I(x) : \Omega \rightarrow R^+, \Omega \subset R^N, N = 3$ and evolve the surface towards the shape boundaries. Applying an analogous argument will elad us to write the following surface evolution equation for $3D$ segmentation:

$$S_t = (gH - \beta(\nabla g \cdot \mathbb{N}))\mathbb{N}, \tag{13}$$

where H is the mean curvature and $\mathbb{N}$ is the normal to the surface.

The curve and surface evolution in Eqns. 12 and 13 can be solved using the level-set approach [20][29] . Consider an $(N-1)$-dimensional hypersurface $\Upsilon(x,t)$ ($N = 2$ for C and $N = 3$ for S) and represent it as the zero level-set of a function $\Psi(x,t) : \Omega \times [0,T] \rightarrow R, \Omega \subset R^N, N = 2,3$. In other words, the initial curve or surface is simply the set $\{\Psi = 0\}$. The function Ψ therefore is and

implicit representation of the hypersurface. Both Eqns. 12 and 13 have the same level-set form, i.e. the main model:

$$\Psi_t = g\left(\nabla \cdot \frac{\nabla\Psi}{|\nabla\Psi|}\right)|\nabla\Psi| + \beta\nabla g \cdot \nabla\Psi$$
$$g(x) = \frac{1}{1 + (|\nabla I_{GS}(x)|/\alpha)^2} \tag{14}$$

with the initial condition $\Psi(x, t = 0) = \Psi_0$. In our case Ψ_0 is the signed distance function from the initial hypersurface $\Upsilon(x, t = 0)$. Note that the function g is an edge indicator expressed as a non-increasing function of the image gradient. The gradient is computed from a geometrically enhanced image, denoted as I_{GS}, using Eqn. 4. This also establishes a link between the two stages of processing we employ in this work. In the next section we show how the image analysis methodology developed in the last two sections can be utilized to build accurate shape descriptions from echocardiograms.

5 $2D$ Echocardiography

Consider a 2D echocardiographic image $I(x)$ from which we want to accurately extract the boundaries of the cardiac chamber. We consider the embedding $\varphi : \Omega \times [0, T] \rightarrow R, \Omega \subset R^2$ and look for the steady state of the evolution equation:

$$\varphi_t = gK|\nabla\varphi| + \beta\nabla g \cdot \nabla\varphi \tag{15}$$
$$g(x) = \frac{1}{1 + (|\nabla I_{GS}(x)|/\alpha)^2} \tag{16}$$

with the initial condition given by a user-defined signed distance function $\varphi(x, 0) = \varphi_0$. The Euclidean curvature K is obtained from the divergence of the unit normal vector:

$$K = \frac{\varphi_{xx}\varphi_y^2 - 2\varphi_x\varphi_y\varphi_{xy} + \varphi_{yy}\varphi_x^2}{(\varphi_x^2 + \varphi_y^2)^{3/2}}. \tag{17}$$

We now show how to approximate the above equation with finite differences. Let us consider a rectangular uniform grid in space-time (t, x, y); then the grid will be the points $(t_n, x_i, y_j) = (n\Delta t, i\Delta x, j\Delta y)$. We use the notation φ_{ij}^n for the value of φ at the grid point (t_n, x_i, y_j). The curvature term is a parabolic contribution to the equation of motion. In terms of numerical scheme we approximate this with central differences. The second term on the right corresponds to pure

passive advection by the underlying velocity field ∇g whose direction and strength depend on position. This term can be approximated through upwind schemes for hyperbolic terms, as noted in [29]. In other words, we check the sign of each component of ∇g and construct one-sided upwind differences in the appropriate direction. We can write now the complete first order scheme to approximate the above equation as

$$\varphi_{ij}^{n+1} = \varphi_{ij}^{n} + \Delta t \left[- \left\{ \begin{array}{c} [g_{ij} K_{ij}^{n} (D_{ij}^{0x^2} + D_{ij}^{0y^2})^{1/2}] \\ [max(g_{ij}^{0x}, 0) D_{ij}^{-x} + min(g_{ij}^{0x}, 0) D_{ij}^{+x} \\ + max(g_{ij}^{0y}, 0) D_{ij}^{-y} + min(g_{ij}^{0y}, 0) D_{ij}^{+y}] \end{array} \right\} \right] \tag{18}$$

where D is a finite difference operator on φ, the superscripts $\{-, 0, +\}$ indicate backward, central and forward differences respectively, and the superscripts $\{x, y\}$ indicate the direction of differentiation. In Figures 6-7, we show the steps involved in the extraction of the heart chamber shape from a noisy echocardiogram. Figure 8 shows the result of ventricular chamber extraction from another echocardiogram data set. Here we make two observations, (1) the algorithm faithfully reconstructs the shape of the heart chamber inspite of large gaps in the edge map, and (2) the algorithm requires the user to place the initial contour reasonably close to the final shape as opposed to mere shape tagging approach described in [17]. This is because we have eliminated the constant inflationary or "edge-seeking" term (Eqn. 2) that was used in [14] to prevent the contour model from propagating past the edge gaps. So, in areas of image with little or no edge information, the length-minimizing curvature term takes over and closes the gap.

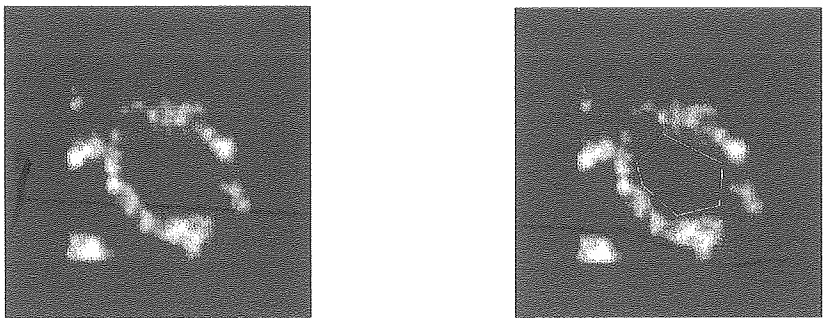

a) b)

Figure 6: *Extraction of the ventricular chamber from a 2D echocardiogram. Left: Initial noisy image with many gaps in the edge description, Right: User defined initial contour expressed as the zero level-set of a function.*

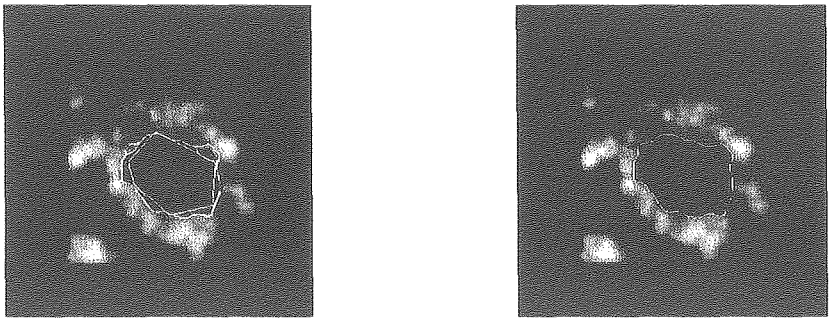

a) b)

Figure 7: *Extraction of the ventricular chamber from a 2D echocardiogram. Left: Various stages of evolutions rendered on the same image, Right: Steady state solution of the level set evolution.*

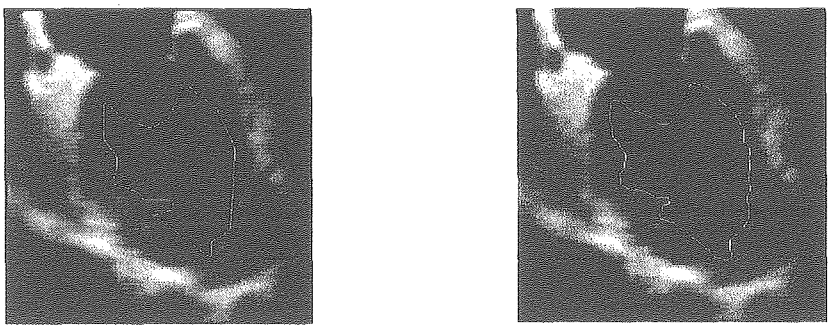

a) b)

Figure 8: *Extraction of the ventricular chamber from a 2D echocardiogram. Left: zero level set of the signed distance function used as initial condition Right: Steady state solution of the level set evolution.*

6 $2D + time$ Echocardiography

The requirement of placing the initial contour reasonably close to the final solution is both restrictive and time consuming. In this section, we address that very issue in the context of analising a time varying sequence of echocardiographic images. Let us now consider a time sequence of $2D$ echocardiographic images that represents an entire cardiac cycle $I^{(m)}, m = 1 \dots M$. We segment the cardiac chamber by extending the geometric model to the time sequence, as follows:

$$\varphi_t^{(m)} = g^{(m)} K^{(m)} |\nabla \varphi^{(m)}| + \beta \nabla g^{(m)} \cdot \nabla \varphi^{(m)} \tag{19}$$

$$g^{(m)}(x) = \frac{1}{1 + (|\nabla I_{GS}^{(m)}(x)|/\alpha)^2} \tag{20}$$

where the initial conditions are $\varphi_0^{(0)} = \varphi_0$ and $\varphi_0^{(m)} = \varphi_{ss}^{(m-1)}, m = 1 \dots M$. That means that for the first frame $m = 0$ the initial condition is a user-defined signed distance function φ_0 and for the subsequent $M-1$ frames the initial condition is automatically given by the steady state solution of the previous frame $\varphi_{ss}^{(m-1)}$. We found that the best results are obtained by considering a starting frame to be the one corresponding to the early diastole, where the mitral valve is completely opened, and to continue the segmentation for half the cardiac cycle in the positive time direction and for the remaining half in the negative time direction, namely:

$$\begin{aligned} \varphi_0^{(M/2)} &= \varphi_0 \\ \varphi_0^{(m)} = \varphi_{ss}^{(m-1)}, m &= (M/2+1) \dots M \\ \varphi_0^{(m-1)} = \varphi_{ss}^{(m)}, m &= (M/2-1) \dots 0 \end{aligned}$$

The result of applying this procedure on a time sequence of $2D$ echocardiographic images is shown in Figures 9-11. In Figures 12-14, we follow the same procedure and show results from a different data set.

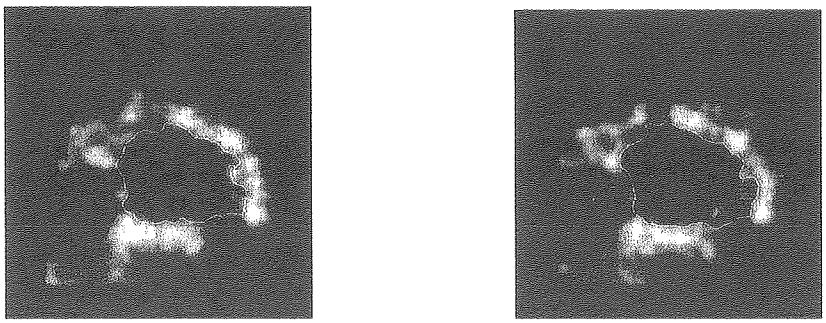

a) b)

Figure 9: *Segmentation of the ventricular chamber from a sequence of time varying echocardiograms. Frames #15 and #16.*

7 $3D$ Echocardiography

We want to accurately extract the $3D$ ventricular shape by retaining the advantages such as easy initialization in $2D$ segmentation and also the regularization properties of a real $3D$ shape extraction

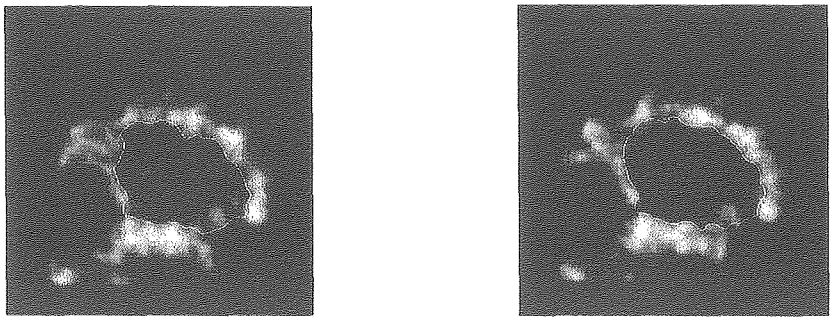

a) b)

Figure 10: *Segmentation of the ventricular chamber from a sequence of time varying echocardiograms. Frames #17 and #18.*

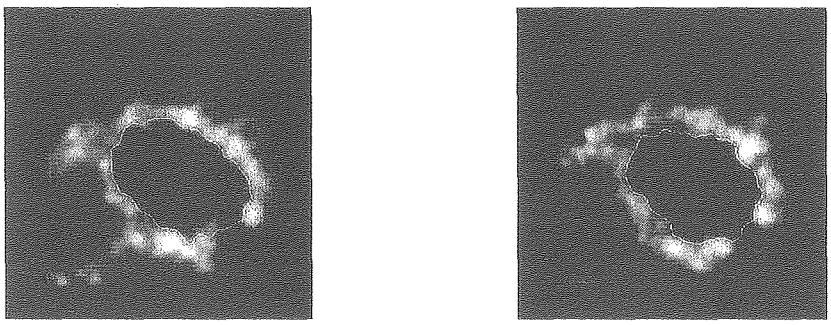

a) b)

Figure 11: *Segmentation of the ventricular chamber from a sequence of time varying echocardiograms. Frames #19 and #20.*

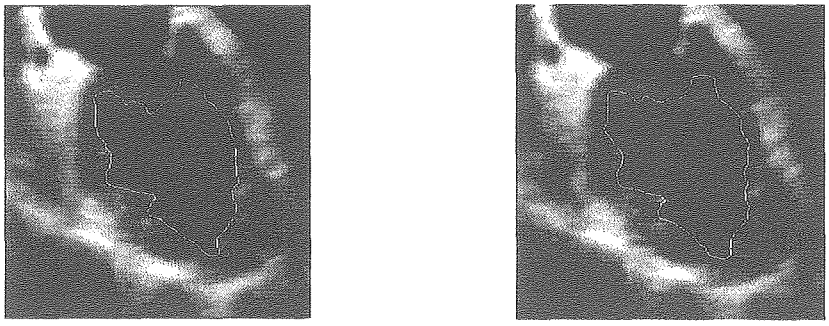

a) b)

Figure 12: *Segmentation of the ventricular chamber from a sequence time varying 2D echocardiographic images. Frames #7 and #8.*

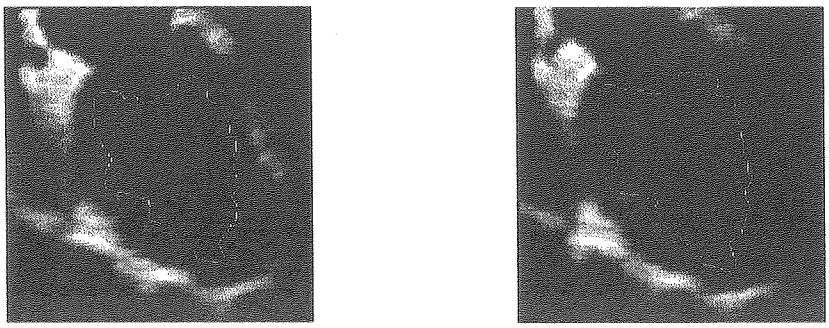

a) b)

Figure 13: *Segmentation of the ventricular chamber from a sequence time varying 2D echocardiographic images. Frames #9 and #10.*

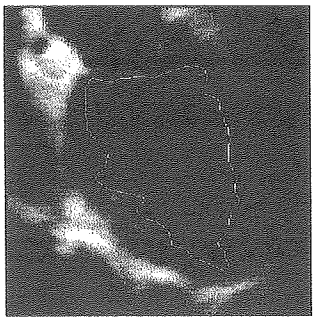

Figure 14: *Segmentation of the ventricular chamber from a sequence time varying 2D echocardiographic images. Frame #11.*

method [16, 17]. We again face the same difficulty that the edge map in $3D$ is both noisy and has many gaps. In addition, in $3D$ it is also problematic for the user to specify an initial model that is reasonably close to the final surface. With this in mind we propose a chain of models to achieve our goal.

First, consider a $3D$ echocardiographic image I_V as a stack of 2-dimensional slices $I_V^{(l)}, l = 0 \ldots L$. As in the $2D + time$ case we apply a sequence of $2D$ segmentation steps using the following model:

$$\varphi_t^{(l)} = g^{(l)} K^{(l)} |\nabla \varphi^{(l)}| + \beta \nabla g^{(l)} \cdot \nabla \varphi^{(l)} \tag{21}$$

$$g^{(l)}(x) = \frac{1}{1 + (|\nabla I_{V_{GS}}^{(l)}(x)|/\alpha)^2} \tag{22}$$

with the initial conditions:

$$\varphi_0^{(l_0)} = \varphi_0$$

$$\varphi_0^{(l)} = \varphi_{ss}^{(l-1)}, l = l_0 \dots L$$
$$\varphi_0^{(l-1)} = \varphi_{ss}^{(l)}, l = l_0 \dots 0$$

where l_0 is a suitable slice. The best results are obtained when l_0 is a long axis view that contains both the mitral valve and the apex. At the end of this stage we have a set of $2D$ contours when stacked on top of each other will provide a good initial guess to start the $3D$ shape extraction problem.

Therefore, we now consider the entire $3D$ image and perform a real $3D$ segmentation by evolving the embedding $\phi : \Omega \times [0,T] \rightarrow R, \Omega \subset R^3$, with the flow:

$$\begin{aligned} \phi_t &= gH|\nabla\phi| + \beta\nabla g \cdot \nabla\phi \\ g(x) &= \frac{1}{1 + (|\nabla I_{V_{GS}}(x)|/\alpha)^2} \end{aligned} \tag{23}$$

with the initial condition given by the union of the previous set of $2D$ segmentation results, i.e. $\phi(0) = U\varphi_{ss}^{(l)}, l = 0 \dots L$.

The mean curvature H can be expressed as a function of the embedding as follows:

$$H = \nabla \cdot \frac{\nabla\phi}{|\nabla\phi|} = \frac{\left\{ \begin{array}{c} (\phi_{yy} + \phi_{zz})\phi_x^2 + (\phi_{xx} + \phi_{zz})\phi_y^2 + (\phi_{xx} + \phi_{yy})\phi_z^2 \\ -2\phi_x\phi_y\phi_{xy} - 2\phi_x\phi_z\phi_{xz} - 2\phi_y\phi_z\phi_{yz} \end{array} \right\}}{(\phi_x^2 + \phi_y^2 + \phi_z^2)^{(3/2)}} \tag{24}$$

To discretize Eqn. 23 consider a uniform grid in space-time (t, x, y, z); then the grid will be the points $(t_n, x_i, y_j, z_k) = (n\Delta t, i\Delta x, j\Delta y, k\Delta z)$. Then the first order scheme that approximates Eqn. 23 is

$$\phi_{ijk}^{n+1} = \phi_{ijk}^n + \Delta t \left[- \left\{ \begin{array}{l} [g_{ijk} H_{ijk}^n (D_{ijk}^{0x^2} + D_{ijk}^{0y^2} + D_{ijk}^{0z^2})^{1/2}] \\ [max(g_{ijk}^{0x}, 0) D_{ijk}^{-x} + min(g_{ijk}^{0x}, 0) D_{ijk}^{+x} \\ +max(g_{ijk}^{0y}, 0) D_{ijk}^{-y} + min(g_{ijk}^{0y}, 0) D_{ijk}^{+y} \\ +max(g_{ijk}^{0z}, 0) D_{ijk}^{-z} + min(g_{ijk}^{0z}, 0) D_{ijk}^{+z}] \end{array} \right\} \right] \tag{25}$$

using the same notation as before. A demonstration of this scheme is shown in Figure 15. The picture on the left is a rendition of the initial surface constructed by assembling all the individual $2D$ contours. This shape is then regularized and drawn towards the $3D$ edge map by solving Eqn. 23 for a few time steps; the result is depicted in the right picture.

Next, we compare the volume measurement we obtain from our $3D$ segmentation to that of experimentally computed values on a couple of sheep heart data sets. The echocardiographic data

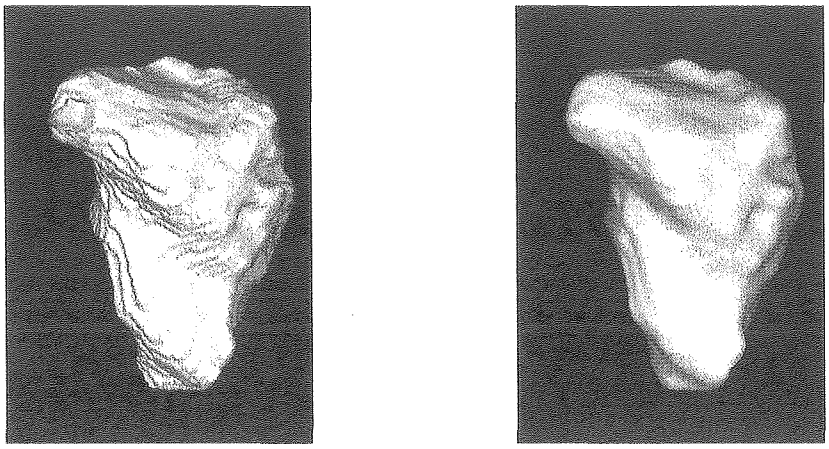

a) b)

Figure 15: *Extraction of the ventricular chamber in 3D echocardiography. Left: segmentation of the 3D image as a spatial sequence of 2D images. Right: full 3D shape refinement.*

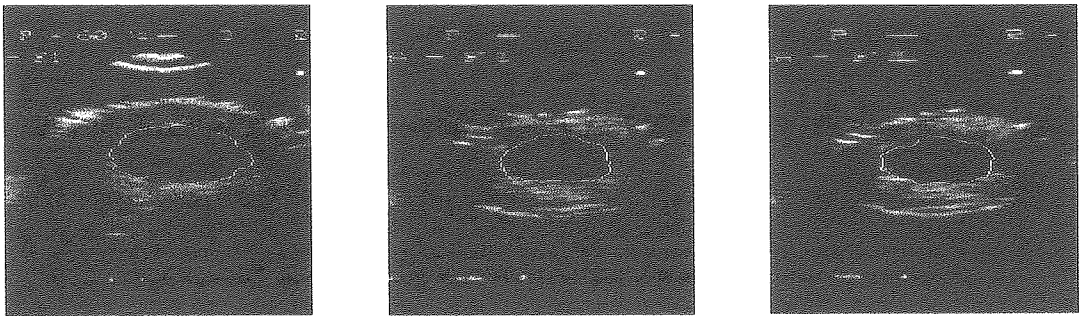

a) b) c)

Figure 16: *Heart shape extraction and volume comparison from 3D images of sheep hearts; see the text.*

was obtained from sheep hearts; for details on data acquisition and experimental heart volume computation, the reader is referred to the work of Pini *et. al* [21, 22]. The volume figures on two sheep hearts according to [21, 22] are 39.0 and 35.7 cm^3, and the volume figures we obtain by first extracting the $3D$ surfaces from corresponding echocardiograms is 42.2 and 35.4 cm^3, i.e. an error of 7.6 % and 0.8 % respectively. Some cross-sections of those surfaces is shown in Figure 16.

8 $3D + time$ Echocardiography

Finally, let us consider a $3D$ sequence of echocardiographic images $I_{VT}^{(m)}, m = 0 \ldots M$. To segment the ventricular shape from the entire sequence, we adopt the same strategy as we did for time

varying $2D$ seqence and apply the following flow:

$$\phi_t^{(m)} = g^{(m)} H^{(m)} |\nabla \phi^{(m)}| + \beta \nabla g^{(m)} \cdot \nabla \phi^{(m)} \tag{26}$$

$$g^{(m)}(x) = \frac{1}{1 + (|\nabla I^{(m)}_{VT_{GS}}(x)|/\alpha)^2} \tag{27}$$

This equation is solved with appropriate initial conditions for each time frame. We applied this scheme to a time varying sequence of echocardiograms and computed the volume of the left ventricular shape while the heart is in a cardiac cycle. The plot of the computed volume is shown in Figure 17. It is now possible to reliably compute quantities like the ejection fraction from noisy echocardiograms.

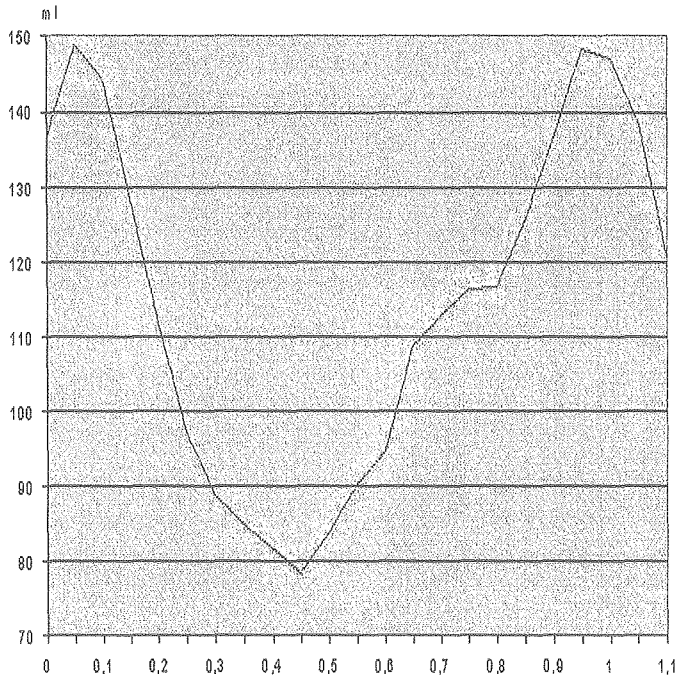

Figure 17: *The plot.*

9 Conclusions

We presented a geometry-based partial differential equation (PDE) approach for filtering and segmentation of echocardiographic images. The method allows edge-preserving image smoothing and a semi-automatic segmentation of the heart chambers. This approach uses regularization to fill in the edge-gaps and improves edge fidelity. A numerical scheme for solving the proposed PDE is

carried out from level set methods. Results on human in vivo acquired $2D$, $2D + time$, $3D$, and $3D + time$ echocardiographic images have been shown.

Acknowledgements

We thank Prof. Pini for giving us the sheep heart data and the volume figures that we used in our comparison.

References

[1] D. Adalsteinsson and J. A. Sethian, "A fast level set method for propagating interfaces," in *J. Comp. Phys.*, Vol. 118(2), pp. 269–277, May 1995.

[2] L. Alvarez, F. Guichard, P. L. Lions, and J. M. Morel, "Axioms and fundamental equations of image processing," *Arch. Rational Mechanics* **123**, 1993.

[3] W. Bommer, L. Weinert, A. Neumann, J. Neef, D. Mason, A. Demaria, *Determination of right atrial and right ventricular size by two-dimensional echocardiography*, Circulation, pp. 60-91 (1979)

[4] V. Caselles, F. Catte. T. Coll, F. Dibos, "A geometric model for active contours," *Numerische Mathematik*, Vol. 66, pp. 1–31, 1993.

[5] V. Caselles, R. Kimmel, and G. Sapiro, "Geodesic active contours," in *Proc. ICCV'95*, Cambridge, MA 1995.

[6] L.D Cohen, *On active contour models and balloons* CVGIP:Image Understanding vol. 53, pag. 211-218.

[7] I. Cohen, L.D Cohen, N. Ayache, *Using deformable surfaces to segment 3D images and infer differential structure* CVGIP:Image Understanding vol. 56, pag. 242-263.

[8] M. Grayson, "The heat equation shrinks embedded plane curves to round points," *J. Differential Geometry* **26**, 1987, pp. 285-314.

[9] A.Handlovičová, K.Mikula, A.Sarti, *Numerical solution of parabolic equations related to level set formulation of mean curvature flow*, Computing and Visualization in Science (1998)

[10] C. Lamberti, F. Sgallari, *Edge detection and velocity field for the analysis of heart motion*, Digital Signal Processing 91, Elsevier (Editors V. Cappellini, A.G. Costantinides) pp. 603-608 (1991)

[11] W.E. Lorensen, H.E. Cline *Marching cubes: a high resolution 3D surface construction algorithm*, Computer Graph., vol. 21, pp. 163-169 (1987)

[12] M. Kass, A. Witkin, D. Terzopoulos, *Snakes: Active contour models*, International Journal of Computer Vision, vol. 1, pp. 321-331, 1988

[13] R. Malladi, J.A. Sethian, B.C. Vemuri, "A topology-independent shape modeling scheme," in *SPIE: Geometric Methods in Computer Vision II*, Vol. 2031, pp. 246–258, 1993.

[14] R. Malladi, J. A. Sethian and B. C. Vemuri, "Shape modeling with front propagation: A level set approach," *IEEE Trans. on PAMI* **17**, 1995, pp. 158-175.

[15] R. Malladi and J. A. Sethian, "Image processing: Flows under Min/Max curvature and mean curvature," in *Graphical Models and Image Processing*, Vol. 58(2), pp. 127–141, March 1996.

[16] R. Malladi and J. A. Sethian, "Level set methods for curvature flow, image enchancement, and shape recovery in medical images," in *Visualization and Mathematics: Experiments, Simulations, and Environments*, Eds. H. C. Hege, K. Polthier, pp. 329–345, Springer Verlag, Heidelberg, 1997.

[17] R. Malladi and J. A. Sethian, "A real-time algorithm for medical shape recovery," in *Proceedings of ICCV '98*, pp. 304–310, Mumbai India, January 1998.

[18] K.Mikula, A.Sarti, C.Lamberti "Geometrical diffusion in 3D echocardiography", *Proc. of ALGORITMY '97- Conference on Scientific Computing*, West Tatra Mountains, Slovakia, 1997.

[19] N. K. Nordstrom, "Variational edge detection," *PhD dissertation* , Department of electrical engineering, University of California, Berkeley, 1990

[20] S. J. Osher and J. A. Sethian, "Fronts propagation with curvature dependent speed: Algorithms based on Hamilton-Jacobi formulations," *Journal of Computational Physics* **79**, 1988, pp. 12-49.

[21] Pini R, Giannazzo G, Di Bari M, Innocenti F, Rega L, Casolo G, and Devereux RB, "Transthoracic three-dimensional echocardiographic reconstruction of left and right ventricles: In vitro validation and comparison with magnetic resonance imaging," *American Heart Journal*, 133: pp. 221–229, 1997.

[22] Pini R, Giannazzo G, Di Bari M, Innocenti F, Marchionni N, Gori A, and Devereux RB, "Left ventricular volume determination by 3-D echocardiographic volume imaging and biplane angiography," *Journal of Noninvasive Cardiology*, 3, pp. 46–51, 1999.

[23] Bart M. ter Haar Romeny(Ed.) *Geometry-driven diffusion in computer vision*, Kluwer Academic Press, 1994.

[24] G. Sapiro, "Color snakes," Hewlett-Packard Lab. tech report, 1995.

[25] G. Sapiro, R. Kimmel, D. Shaked, B. B. Kimia, and A. M. Bruckstein, "Implementing continuous-scale morphology via curve evolution," *Pattern Recognition*, Vol. 26(9), pp. 1363–1372, 1993.

[26] A.Sarti, K.Mikula, F.Sgallari "Nonlinear multiscale analysis of 3D echocardiographic sequences", Submitted to *IEEE Trans. on Medical Imaging*, 1998.

[27] A. Sarti, C. Ortiz de Solorzano, S. Lockett, and R. Malladi, "Computer-Aided Cytology: A Geometric Model for $3D$ Confocal Image Analysis," submitted to *IEEE Transactions of Biomedical Engineering*, March 1999.

[28] J. A. Sethian, "A review of recent numerical algorithms for hypersurfaces moving with curvature dependent flows," *J. Differential Geometry* **31**, 1989, pp. 131-161.

[29] J. A. Sethian, *Level set methods: Evolving interfaces in geometry, fluid mechanics, computer vision, and material science*, Cambridge University Press, 1997.

[30] W. Shroeder, K. Martin, B. Lorensen, *The visualization Toolkit*, Prentice Hall PTR., New Jersey (1996)

[31] S.Shutilov, *Fundamental Physics of Ultrasounds*, Gordon and Breach , New York, 1988

[32] N. Sochen, R. Kimmel, and R. Malladi, "A General Framework for Low Level Vision," in *IEEE Transactions on Image Processing*, special issue on PDEs and Geometry-Driven Diffusion in Image Processing and Analysis, Vol. 7, No. 3, pp. 310–318, March 1998.